



Fu, G., Sing, D. K., Deming, D., Sheppard, K., Wakeford, H. R., Mikal-Evans, T., Alam, M. K., Dos Santos, L. A., López-Morales, M., & Lothringer, J. D. (2022). The Hubble PanCET Program: Emission Spectrum of Hot Jupiter HAT-P-41b. *The Astronomical Journal*, 163(4), [190]. <https://doi.org/10.3847/1538-3881/ac58fc>

Publisher's PDF, also known as Version of record

License (if available):  
CC BY

Link to published version (if available):  
[10.3847/1538-3881/ac58fc](https://doi.org/10.3847/1538-3881/ac58fc)

[Link to publication record in Explore Bristol Research](#)  
PDF-document

This is the final published version of the article (version of record). It first appeared online via IOP at [10.3847/1538-3881/ac58fc](https://doi.org/10.3847/1538-3881/ac58fc) . Please refer to any applicable terms of use of the publisher.

## University of Bristol - Explore Bristol Research

### General rights

This document is made available in accordance with publisher policies. Please cite only the published version using the reference above. Full terms of use are available: <http://www.bristol.ac.uk/red/research-policy/pure/user-guides/ebr-terms/>



# The Hubble PanCET Program: Emission Spectrum of Hot Jupiter HAT-P-41b

Guangwei Fu<sup>1</sup> , David K. Sing<sup>2</sup> , Drake Deming<sup>1</sup>, Kyle Sheppard<sup>1</sup> , H. R. Wakeford<sup>3</sup> , Thomas Mikal-Evans<sup>4</sup> ,  
Munazza K. Alam<sup>5</sup> , Leonardo A. Dos Santos<sup>6,7</sup> , Mercedes López-Morales<sup>8</sup> , and Joshua D. Lothringer<sup>9</sup>

<sup>1</sup>Department of Astronomy, University of Maryland, College Park, MD 20742, USA; [guangweifu@gmail.com](mailto:guangweifu@gmail.com)

<sup>2</sup>Department of Physics and Astronomy, Johns Hopkins University, Baltimore, MD 21218, USA

<sup>3</sup>School of Physics, University of Bristol, HH Wills Physics Laboratory, Tyndall Avenue, Bristol BS8 1TL, UK

<sup>4</sup>Department of Physics, and Kavli Institute for Astrophysics and Space Research, Massachusetts Institute of Technology, Cambridge, MA, USA

<sup>5</sup>Carnegie Earth & Planets Laboratory, 5241 Broad Branch Road NW, Washington, DC 20015, USA

<sup>6</sup>Observatoire astronomique de l'Université de Genève, Chemin Pegasi 51, 1290 Versoix, Switzerland

<sup>7</sup>Space Telescope Science Institute, 3700 San Martin Drive, Baltimore, MD 21218, USA

<sup>8</sup>Center for Astrophysics | Harvard & Smithsonian, 60 Garden Street, Cambridge, MA 02138, USA

<sup>9</sup>Department of Physics, Utah Valley University, Orem, UT, USA

Received 2021 October 14; revised 2022 February 17; accepted 2022 February 24; published 2022 March 25

## Abstract

We present the most complete emission spectrum for inflated hot Jupiter HAT-P-41b combining new Hubble Space Telescope Wide Field Camera/G141 spectrum from the Hubble Panchromatic Comparative Exoplanet Treasury program with archival Spitzer eclipse observations. We found a near blackbody-like emission spectrum, which is best fitted with an isothermal temperature–pressure (TP) profile, that agrees well with the dayside heat redistribution scenario assuming zero Bond albedo. The noninverted TP profile is consistent with the nondetection of near-UV/optical absorbers in the transit spectra. We do not find any evidence for significant H<sup>−</sup> opacity nor a metal-rich atmosphere. HAT-P-41b is an ideal target that sits in the transitioning parameter space between hot and ultra-hot Jupiters, and future James Webb Space Telescope observations will help us to better constrain the thermal structure and chemical composition.

*Unified Astronomy Thesaurus concepts:* [Exoplanet atmospheres \(487\)](#)

## 1. Introduction

Emission spectroscopy of exoplanets allows us to probe into the deeper layers (1–10 bar) of the dayside atmosphere compared to transmission spectroscopy which measures the upper layers (~1 mbar) of the planetary limbs. The difference in the radiative transfer path geometry means that the emission spectrum is much more sensitive to the vertical thermal structure of the planet. Depending on the atmospheric chemical composition and the temperature–pressure (TP) profile, molecular absorption, or emission features can be imprinted onto the emission spectrum. Notably, water features at 1.4  $\mu\text{m}$  (Fu et al. 2017) have been the most robustly detected in both absorption (Kreidberg et al. 2014) and emission (Evans et al. 2017; Fu et al. 2022). The presence of H<sup>−</sup> continuum opacity was inferred in multiple ultra-hot Jupiters (Arcangeli et al. 2019; Fu et al. 2021a). In the longer wavelength, the CO/CO<sub>2</sub> features were indicated by the deviations of Spitzer photometric points in the 3.6 and 4.5  $\mu\text{m}$  channels from the blackbody approximation (Garhart et al. 2020; Fu et al. 2021b).

HAT-P-41b is an inflated hot Jupiter ( $R = 1.685^{+0.076}_{-0.051} R_{\text{Jup}}$ ,  $M = 0.8^{+0.1}_{-0.1} M_{\text{Jup}}$ ,  $T_{\text{eq}} = 1940^{+38}_{-38} \text{K}$ ; Hartman et al. 2012) with detailed atmospheric characterization via transmission spectroscopy (Lewis et al. 2020; Wakeford et al. 2020; Sheppard et al. 2021). The planet shows a high-metallicity (Wakeford et al. 2020; Sheppard et al. 2021) atmosphere with an increased H<sup>−</sup> opacity abundance (Lewis et al. 2020). With a dayside temperature of ~2300 K, HAT-P-41b sits between hot and ultra-hot Jupiters where physical processes such as

molecular dissociation and H<sup>−</sup> opacity are starting to become important (Parmentier et al. 2018). HAT-P-41b allows us to pinpoint the transitional parameter space of various atmospheric processes which makes it a valuable data point in our understanding of hot-Jupiter atmospheres on a population level (Baxter et al. 2021; Mansfield et al. 2021). Here we present the 1.1 to 4.5  $\mu\text{m}$  emission spectrum of HAT-P-41b with combined data from Hubble Space Telescope (HST)/Wide Field Camera 3 (WFC3) G141 and Spitzer channel 1 and 2.

## 2. Observations

The HST WFC3/G141 data set was observed as a part of the Panchromatic Exoplanet Treasury Survey (PanCET GO 14767; PIs: Sing & Lopez-Morales) on 2016 October 9 and the Spitzer data set was published in Garhart et al. (2020). The WFC3/G141 eclipse observation was taken in spatial scan mode for five consecutive HST orbits. Each frame was taken with the 256 × 256 pixel subarray in the SPARS10 and NSAMP = 12 settings. The forward scanning rate is 0.065 s<sup>−1</sup> and the exposure time is 81 s.

## 3. HST WFC3 Data Reduction

All the orbital parameters for the WFC3/G141 data reduction have been fixed to the same values used in Sheppard et al. (2021) which are identical to what were used in the (Garhart et al. 2020) Spitzer analysis.

The data reduction process starts with applying the standard flat-field, background subtraction, and bad pixels, as well as the cosmic ray removal on the ima frames (Fu et al. 2021a). Then we extract the nondestructive reads from each frame (Deming et al. 2013). There is a spatially resolved companion star (Sheppard et al. 2021) located 3.6" away. Due to the large



Original content from this work may be used under the terms of the [Creative Commons Attribution 4.0 licence](#). Any further distribution of this work must maintain attribution to the author(s) and the title of the work, journal citation and DOI.

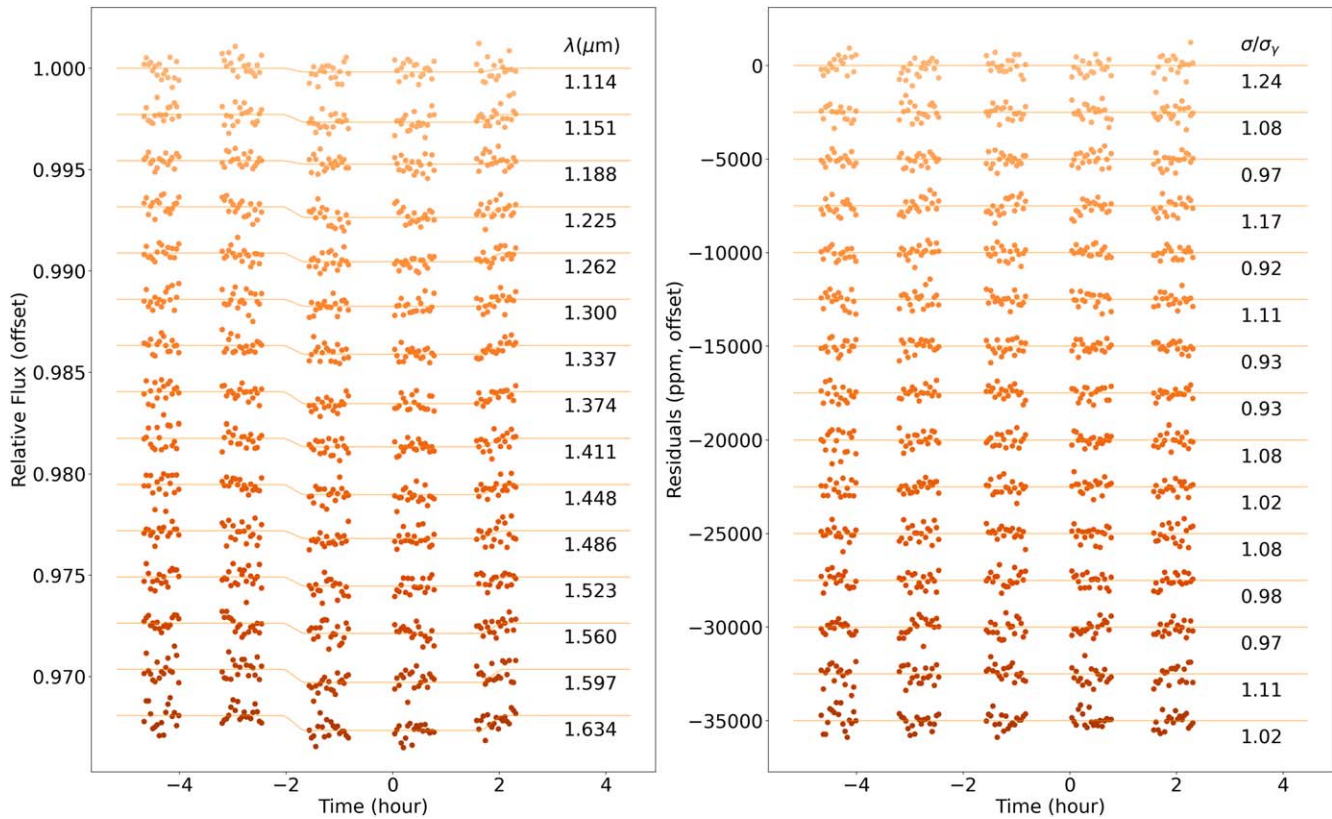


**Figure 1.** HST WFC3 G141 spectral bin transit lightcurves after ramp-effect correction using RECTE (left) and corresponding residuals (right) with their relative ratios to the photon-limit noise ( $\sigma/\sigma_\gamma$ ) levels.

spatial separation, the nondestructive reads of the spatial scan from the two stars do not overlap which allows for clean removal of the companion star spectra. The companion star removed reads are then combined to the complete spatial scan frames. Next we summed each frame in the vertical direction for the 1D spectrum and normalized it by its own median flux to calculate the wavelength shifts. We then used the *scipy.interpolate.interp1d* function to interpolate the 1D spectrum in the wavelength direction and calculated the relative subpixel level shifts of each frame. The largest shift between any two frames is under 0.1 pixel which does not induce any excessive systematics (Stevenson & Fowler 2019). Wavelength shifts corrected non-normalized frames were then summed in all wavelength channels to form the white light eclipse lightcurve. The lightcurve is then fitted with a combination of BATMAN (Kreidberg 2015) with the RECTE charge trapping systematics model (Zhou et al. 2017), second order polynomial of the HST orbital phase, and the wavelength shifts. Each wavelength channel is then fitted using the same method but with the midtransit time fixed to the best-fit white light value. The best-fit lightcurves of each wavelength channel and corresponding residuals are shown in Figure 1. We also compared our spectrum with that in Mansfield et al. (2021) and they are in good agreement (Figure 2).

#### 4. Retrieval Analysis

We performed the retrieval analysis on the reduced HAT-P-41b emission spectrum with ATMO (Amundsen et al. 2014; Tremblin et al. 2015; Drummond et al. 2016; Tremblin et al. 2016; Wakeford et al. 2017; Goyal et al. 2018). The retrieval setup is equilibrium chemistry with a fixed solar C/O ratio.

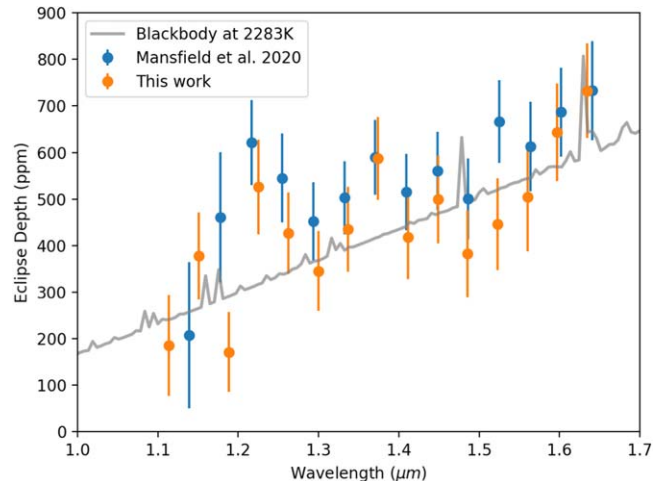


**Figure 2.** The WFC3/G141 emission spectrum is in excellent agreement with that in Mansfield et al. (2021).

There is a total of four free fitting parameters (Table 1) including metallicity ( $Z$ ) and three parameters  $\kappa_{\text{IR}}$ ,  $\gamma_{\text{O/IR}}$ , and  $\beta$  for the TP profile as defined in Line et al. (2013). We fixed the C/O ratio to the solar value due to the lack of constraint this data set has on the carbon-bearing species. Also, the transit spectra retrieval (Lewis et al. 2020; Sheppard et al. 2021) results were all consistent with the solar C/O values.

The best-fit model to the emission spectrum (Table 2) from the ATMO retrieval (Figure 3) gives a  $\chi^2_\nu$  of 1.24 (4 degrees of freedom) with a near-isothermal TP profile. The best-fit blackbody temperature using the PHOENIX stellar model (Husser et al. 2013) grid ( $\log g = 4.5$  and  $\log Z = 0$ ) interpolated

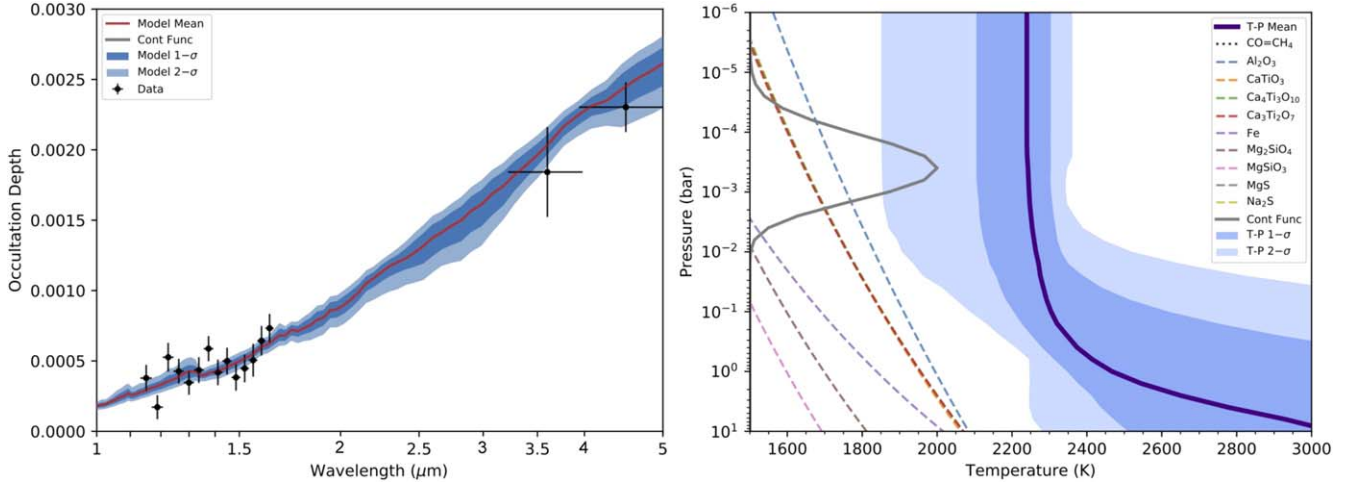


**Figure 3.** ATMO retrieval of the HAT-P-41b emission spectrum. The featureless black-like spectrum (left) is best fitted with an isothermal TP profile (right).

**Table 1**  
ATMO Eclipse Retrieval Priors and Posteriors

Parameter	Priors	Posteriors
$\log(Z/Z_{\odot})$	$\mathcal{U}(-2.8, 2.8)$	$-0.342^{+1.677}_{-1.277}$
$\log(K_{\text{IR}})$	$\mathcal{U}(-5, -0.5)$	$-2.887^{+0.982}_{-0.907}$
$\log(\gamma_{\text{IR}})$	$\mathcal{U}(-4, 1.5)$	$-0.907^{+0.672}_{-1.716}$
beta	$\mathcal{U}(0, 2)$	$1.326^{+0.068}_{-0.168}$

to  $T_{\text{eff}} = 6390 \text{ K}$  is  $2283 \pm 64 \text{ K}$  with a  $\chi^2_{\nu}$  of 1.23 (1 degree of freedom). Based on the formalism described in Cowan & Agol (2011), this dayside temperature would suggest a circulation efficiency  $\varepsilon$  of 0.44 assuming zero Bond albedo and the predicted nightside temperature would be 1572 K.  $\varepsilon = 0$  represents the noncirculation limit where the nightside temperature is 0 K and  $\varepsilon = 1$  represents the full-circulation scenario where the nightside temperature is the same as the dayside. The measured dayside temperature is consistent with the dayside-only heat redistribution scenario. The retrieved metallicity is consistent with the solar value (Figure. 4). While Sheppard et al. (2021) retrieved metallicity  $\sim 1\sigma$  higher than solar, Lewis et al. (2020) reported values consistent with solar metallicity. Considering the large uncertainties on metallicity from all three studies, the current data sets cannot well constrain the models.

Lewis et al. (2020) found H- abundance several orders of magnitude larger than equilibrium chemistry is needed to best fit the transmission spectrum. We did not find evidence for significant H<sup>-</sup> opacity from the emission spectrum and we believe this could be due to the following: (1) The blackbody-like emission spectrum and near-isothermal TP profile make the abundances largely unconstrained. (2) The H<sup>-</sup> constrain in Lewis et al. (2020) comes from a combination of WFC3 G280 and G141 data. Wakeford et al. (2020) did not find evidence for H<sup>-</sup> solely based on the G280 optical data set. Therefore any uncorrected offsets between G280 and G141 spectra can potentially lead to high H<sup>-</sup> abundance. (3) Sheppard et al. (2021) did not retrieve significant H<sup>-</sup> abundance with both G280 and G141 data sets using a different retrieval code. So it could also be due to different forward model assumptions.

Heavy metals such as Fe I, Fe II, and molecules like TiO are considered major optical absorbers that can induce temperature

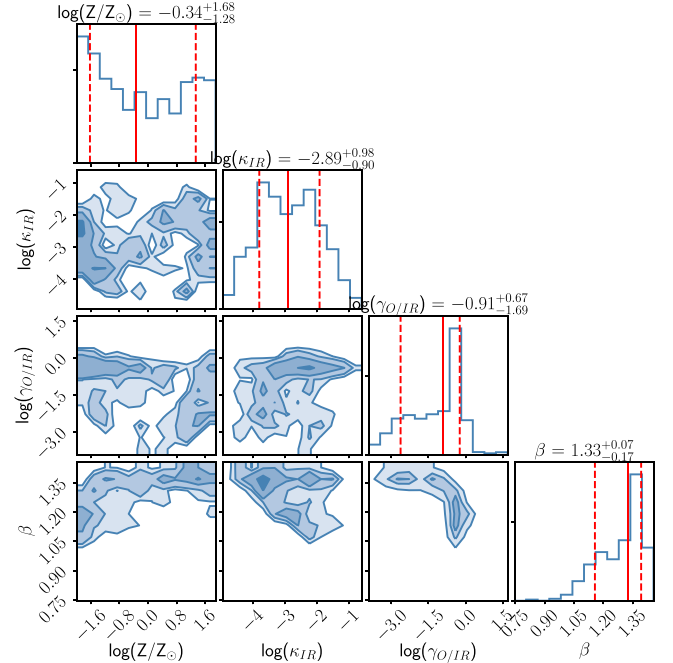


**Figure 4.** Posterior distribution of the ATMO retrieval. The metallicity is mostly unconstrained due to a lack of features within the emission spectrum.

inversion in hot-Jupiter atmospheres (Fortney et al. 2008; Lothringer et al. 2020), and they have been detected in the optical transit spectrum with HST/STIS G430L and G750L (Fu et al. 2021a). There are no significant near-UV heavy metals nor optical TiO absorption detected in both the Space Telescope Imaging Spectrograph (STIS; Sheppard et al. 2021) and Ultraviolet Imaging Spectrograph (UVIS; Lewis et al. 2020; Wakeford et al. 2020) transmission spectra for HAT-P-41b. The noninverted TP profile retrieved in this HAT-P-41b emission spectrum is consistent with the nondetection of near-UV/optical absorbers in the transit spectra.

## 5. Compared with Other Hot-Jupiter Atmospheres

To quantify the WFC3/G141 emission spectra from various hot Jupiters and compare HAT-P-41b to them, we took the  $1.4 \mu\text{m}$  water feature strength index ( $S_{\text{H}_2\text{O}}$ ) reported in

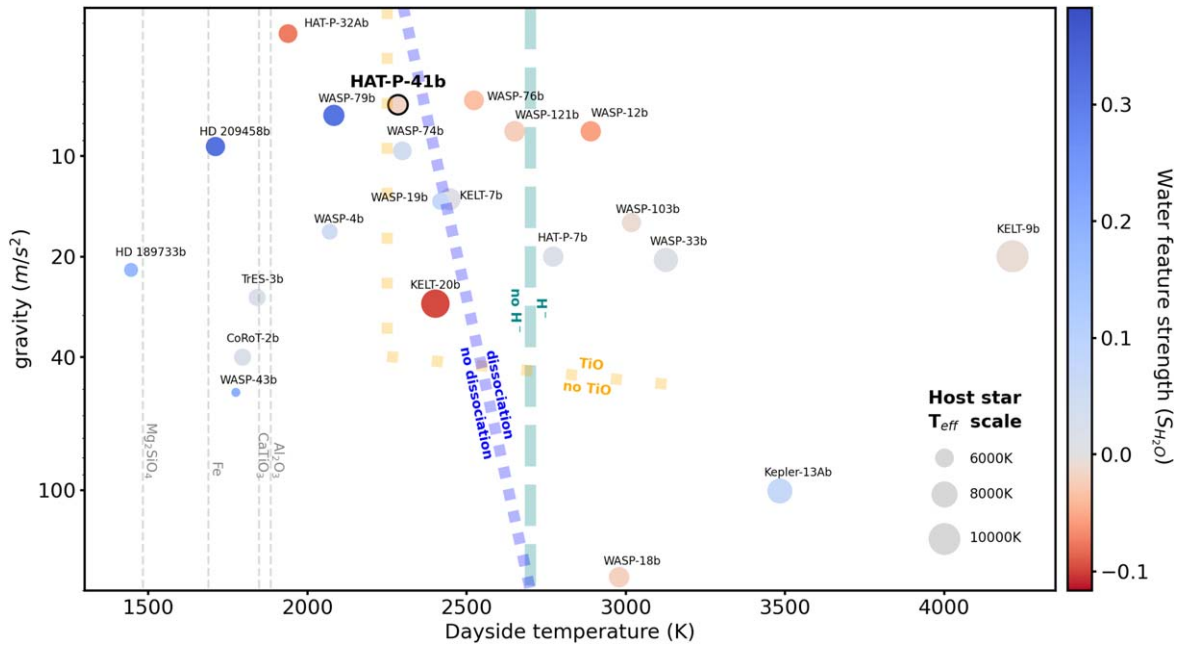


**Figure 5.** HAT-P-41b WFC3/G141 emission spectrum compared with other hot Jupiters. The water feature strength index ( $S_{\text{H}_2\text{O}}$ ; Mansfield et al. 2021) measures the  $1.4 \mu\text{m}$  water band feature size relative to the blackbody model based on the out-of-band spectrum. Centered at zero, with zero being the blackbody-like featureless spectrum. Increasing negative values (redder color) represent stronger emission features and increasing positive values (bluer color) represent stronger absorption features. The circle size scales with the host star temperature ( $T_{\text{eff}}$ ). The gray vertical dash lines are condensation lines for various metals at 100 mbar assuming solar metallicity. We see mostly featureless spectra at higher dayside temperatures ( $>2700 \text{ K}$ ) where  $\text{H}^-$  continuum opacity expects to dominate (Parmentier et al. 2018). At the lower temperature side, we see mostly water absorption features where the atmosphere is too cool for gaseous heavy metal absorbers such as  $\text{TiO}$  to form and drive thermal inversion. HAT-P-41b sits at this in between transitional region where planets can have absorption, emission, or featureless spectra. Further observations of HAT-P-41b in the longer wavelength with the James Webb Space Telescope (JWST) will help us to precisely determine its thermal structure and understand what causes thermal inversion in hot-Jupiters atmospheres.

Mansfield et al. (2021) and plotted them in the dayside temperature versus gravity parameter space (Figure 5) first introduced in Parmentier et al. (2018). The important physical transitions including  $\text{TiO}$ ,  $\text{H}^-$ , and molecular dissociation are also the same as shown in Parmentier et al. (2018). The larger negative  $S_{\text{H}_2\text{O}}$  values (redder) represent stronger water emission features while the larger positive values (bluer) indicate more prominent water absorption features. The index is centered at zero for a blackbody-like featureless spectrum. In addition, we also scale the size of each point based on the host star temperature ( $T_{\text{eff}}$ ) to reflect the effect of increased far-UV/UV radiations from earlier type stars (Lothringer & Barman 2019; Fu et al. 2022).

We have only seen strong water absorption features among cooler hot-Jupiter ( $T_{\text{day}} < 2200 \text{ K}$ ) atmospheres (Kreidberg et al. 2014; Line et al. 2016) driven by their decreasing TP profiles. This is due to heavy metal absorbers condensing out of the atmosphere at low temperatures. On the other hand, when the atmosphere becomes too hot ( $T_{\text{day}} > 2700 \text{ K}$ ), water molecules dissociate and  $\text{H}^-$  continuum opacity starts to dominate. As a result, we have only observed featureless emission spectra among the hottest planets. In between the two regions ( $\sim 2200$  to  $2700 \text{ K}$ ) we see a transitional parameter space where atmospheres can be inverted (Evans et al. 2017; Fu et al. 2022) or isothermal (Fu et al. 2021b; Mansfield et al. 2021). HAT-P-41b sits in the middle of this transitional space. Its mostly featureless WFC3/G141 emission spectrum is similar to that of WASP-76b, WASP-74b, WASP-19b, and KELT-7b. However, it is different from WASP-121b and KELT-20b where we saw evidence for water emissions. Although previous models have indicated multiple important

**Table 2**  
HAT-P-41b Eclipse Spectrum

Wavelength Mid-point ( $\mu\text{m}$ )	Bin Width ( $\mu\text{m}$ )	Occultation Depth (ppm)	Uncertainty (ppm)
1.1137	0.0186	186	108
1.1509	0.0186	378	94
1.1881	0.0186	171	86
1.2253	0.0186	526	102
1.2625	0.0186	427	87
1.2997	0.0186	346	86
1.3369	0.0186	435	91
1.3741	0.0186	587	89
1.4113	0.0186	419	91
1.4485	0.0186	499	95
1.4857	0.0186	383	94
1.5229	0.0186	446	99
1.5601	0.0186	505	117
1.5973	0.0186	643	105
1.6345	0.0186	733	102
3.6000	0.3800	1842	319
4.5000	0.5600	2303	177





physical transitions (Parmentier et al. 2018) happening at this temperature and gravity range, it is not yet well understood what exact physical processes drive the different thermal structures and emission spectra of these planets. In addition, host star type could be another important determining factor since strong far-UV/UV radiations from the host star can strengthen atmospheric thermal inversion (Lothringer & Barman 2019; Fu et al. 2022) as they deposit significant energy into the upper layers of the planetary atmospheres. This is






supported by the large emission features seen in KELT-20b which orbits an A-type star. The lack of far-UV/UV flux from F-type host star of HAT-P-41b could be another cause for its isothermal atmosphere.

## 6. Conclusion

We present the most complete emission spectrum for inflated hot Jupiter HAT-P-41b. The spectrum is close to blackbody-like with no significant molecular absorption or emission features. The best-fit ATMO model shows an isothermal TP profile agreeing with the dayside heat redistribution scenario and a metallicity value consistent with the solar value. The noninverted TP profile is consistent with the nondetection of near-UV/optical absorbers in the transit spectra. Significant  $H^-$  opacity suggested in Lewis et al. (2020) is not required in the model to adequately fit the emission spectrum. We also do not retrieve a metal-rich atmosphere as indicated in Sheppard et al. (2021). However, the emission spectrum does not well constrain the atmosphere metallicity due to the limited wavelength coverage. The featureless emission spectrum of HAT-P-41b indicates planets with dayside temperatures around 2300 K may have relatively isothermal TP profiles in the absence of heavy metal absorbers and strong host star far-UV/UV radiations to drive thermal inversion. The comparison of HAT-P-41b to other similar hot Jupiters paints a murky picture of how atmospheric physical properties transition from cooler to hotter planets. The combined effect of surface gravity, thermal dissociation,  $H^-$  opacity, heavy metal absorbers, and host star type is yet to be disentangled. Future observations of more similar planets and follow-up JWST infrared measurements of HAT-P-41b will be the key to solving the mystery of hot-Jupiter atmospheres.

## ORCID iDs

Guangwei Fu  <https://orcid.org/0000-0002-3263-2251>  
 David K. Sing  <https://orcid.org/0000-0001-6050-7645>  
 Kyle Sheppard  <https://orcid.org/0000-0003-4552-9541>  
 H. R. Wakeford  <https://orcid.org/0000-0003-4328-3867>

Thomas Mikal-Evans  <https://orcid.org/0000-0001-5442-1300>  
 Munazza K. Alam  <https://orcid.org/0000-0003-4157-832X>  
 Leonardo A. Dos Santos  <https://orcid.org/0000-0002-2248-3838>  
 Mercedes López-Morales  <https://orcid.org/0000-0003-3204-8183>  
 Joshua D. Lothringer  <https://orcid.org/0000-0003-3667-8633>

## References

- Amundsen, D. S., Baraffe, I., Tremblin, P., et al. 2014, *A&A*, 564, A59  
 Arcangeli, J., Desert, J.-M., Parmentier, V., et al. 2019, *A&A*, 625, A136  
 Baxter, C., Désert, J.-M., Tsai, S.-M., et al. 2021, *A&A*, 648, 39  
 Cowan, N. B., & Agol, E. 2011, *ApJ*, 729, 54  
 Deming, D., Wilkins, A., McCullough, P., et al. 2013, *ApJ*, 774, 95  
 Drummond, B., Tremblin, P., Baraffe, I., et al. 2016, *A&A*, 594, A69  
 Evans, T. M., Sing, D. K., Kataria, T., et al. 2017, *Natur*, 548, 58  
 Fortney, J., Lodders, K., Marley, M., & Freedman, R. 2008, *ApJ*, 678, 1419  
 Fu, G., Deming, D., Knutson, H., et al. 2017, *ApJL*, 847, L22  
 Fu, G., Deming, D., Lothringer, J., et al. 2021a, *AJ*, 162, 108  
 Fu, G., Deming, D., May, E., et al. 2021b, *AJ*, 162, 271  
 Fu, G., Sing, D. K., Lothringer, J. D., et al. 2022, *ApJL*, 925, L3  
 Garhart, E., Deming, D., Mandell, A., et al. 2020, *AJ*, 159, 137  
 Goyal, J. M., Mayne, N., Sing, D. K., et al. 2018, *MNRAS*, 474, 5158  
 Hartman, J. D., Bakos, G., Béky, B., et al. 2012, *AJ*, 144, 139  
 Husser, T.-O., Wende-von Berg, S., Dreizler, S., et al. 2013, *A&A*, 553, A6  
 Kreidberg, L. 2015, *PASP*, 127, 1161  
 Kreidberg, L., Bean, J. L., Désert, J.-M., et al. 2014, *ApJL*, 793, L27  
 Lewis, N. K., Wakeford, H. R., MacDonald, R. J., et al. 2020, *ApJL*, 902, L19  
 Line, M. R., Stevenson, K. B., Bean, J., et al. 2016, *AJ*, 152, 203  
 Line, M. R., Wolf, A., Zhang, X., et al. 2013, *ApJ*, 775, 137  
 Lothringer, J. D., & Barman, T. 2019, *ApJ*, 876, 69  
 Lothringer, J. D., Fu, G., Sing, D. K., & Barman, T. S. 2020, *ApJL*, 898, L14  
 Mansfield, M., Line, M. R., Bean, J. L., et al. 2021, *NatAs*, 5, 1224  
 Parmentier, V., Line, M. R., Bean, J. L., et al. 2018, *A&A*, 617, A110  
 Sheppard, K. B., Welbanks, L., Mandell, A., et al. 2021, *AJ*, 161, 51  
 Stevenson, K. B., & Fowler, J. 2019, Instrument Science Report, *WFC3* 2019-12  
 Tremblin, P., Amundsen, D. S., Chabrier, G., et al. 2016, *ApJL*, 817, L19  
 Tremblin, P., Amundsen, D. S., Mourier, P., et al. 2015, *ApJL*, 804, L17  
 Wakeford, H. R., Sing, D. K., Kataria, T., et al. 2017, *Sci*, 356, 628  
 Wakeford, H. R., Sing, D. K., Stevenson, K. B., et al. 2020, *AJ*, 159, 204  
 Zhou, Y., Apai, D., Lew, B. W. P., & Schneider, G. 2017, *AJ*, 153, 243